

Limits of 3-D nanostructures fabricated by focused electron beam (FEB) induced deposition

P. Hoffmann, I. Utke, and F. Cicoira

Institute of Imaging and Applied Optics, School of Engineering (STI), Ecole Polytechnique Fédérale de Lausanne,
CH-1015 Lausanne-EPFL, Switzerland

Abstract. The focused electron beam of an electron microscope (SEM or TEM) decomposes tailored precursor molecules on substrates into functional deposits. Extremely high aspect ratios of more than 10 can easily be obtained. During the last years several materials could be deposited, most of them composed of metal nanoparticles embedded in amorphous matrices. The deposition process depends on the precursor supply, its surface adsorption behavior, and the beam induced chemical decomposition path of the molecule on one hand, and on the other hand on the electron beam properties like beam current, electron energy, and beam distribution. The limits in minimal size, growth rate, and chemical composition arise from all mentioned parameters, which are interdependent.

Introduction

Since the first "contamination" carbon deposits with a broad [1] and a focused [2] electron beam, several attempts were made to improve the focused electron beam (FEB) induced deposition process with respect to high resolution and deposit purity. Pioneers in the field of metal containing deposits are Matsui and Mori [3] and Koops and coworkers [4, 5]. The physical understanding of FEB deposition was strongly improved by models of Christy [6], Scheuer and Koops [5] and Reimer [7], describing the process as decomposition of surface adsorbed molecules by secondary electrons (SE). One can divide the limiting factors of the process into physical, physico-chemical, and chemical contributions. As physical factors we consider the primary electron beam distribution as well as the resulting secondary electron distribution. They are predominantly responsible for the minimal structure size of the deposits. Physico-chemical parameters are transport phenomena like effusion of molecules, surface diffusion rate, residence time, desorption rate, and adsorption enthalpy. They determine mainly the processing speed, i.e. the maximum deposition rate. The chemical contributions taking place like electron beam induced ionization and fragmentation, thermal decomposition reactions and surface catalyzed decomposition are less known compared to the above mentioned physical and physico-chemical parameters, but are responsible for the chemical composition, i.e. purity, and thus for deposit functionality. During the last years we tried to extend the understanding of FEB induced deposition using novel carbon free precursors like AuClPF₃ and Rh₂Cl₂(PF₃)₄. Our system comprises a SEM (Cambridge S 100) with a thermionic tungsten filament as electron emitter and an oil free pumping system, allowing to study deposition in an electron energy range of 2 – 25 keV and with beam currents of several nA down to 5 pA.

1. Physical properties – Size limits – Electron probe size – Secondary Effects

Generally, FEB deposition electron microscopes have electron energies ranging from several hundreds of eV up to several hundreds of keV. The focused electron beam diameter and its electron distribution are described by a gaussian shaped beam increasing its diameter with increasing current according to fig. 1a. Depending on emitter and electron optics one obtains a distribution of electrons down to several nanometers spot size. It is straightforward that the electron beam distribution will be one important limiting factor for the smallest lateral dimensions that can be obtained. However, electron microscope resolution does not correspond 1:1 to the electron beam diameter because contrast filters allow for additional confinement of the obtained secondary or transmitted electron images. Alternatively, the knife-edge method for beam distribution measurements is complicated due to effects of partial primary electron transmission and increased edge emission of secondary electrons.

We applied short time exposures for deposition of Rhodium containing nano-composite on thin carbon films, see fig. 1b. With decreasing time the deposit diameter saturates at a value corresponding to the knife-edge measured beam diameter. The deposit thickness profile was measured ex-situ by TEM and shows a gaussian shape at the outer deposit region. The central part of the deposits is flat since deposition is precursor flux limited, as will be discussed in the next chapter. The advantage of deposition on thin carbon films is that it avoids generation of backscattered electrons and electromagnetic radiation (X-rays) due to the low excitation volume. If plane bulk substrates are used backscattered electrons result in thin "halo" deposits around the principal deposit [8]. On non-planar substrates as shown in fig. 1c the bottom, shank, and apex diameter of tip deposits can be distinguished. The tip apex diameter corresponds to the measured beam diameter (at

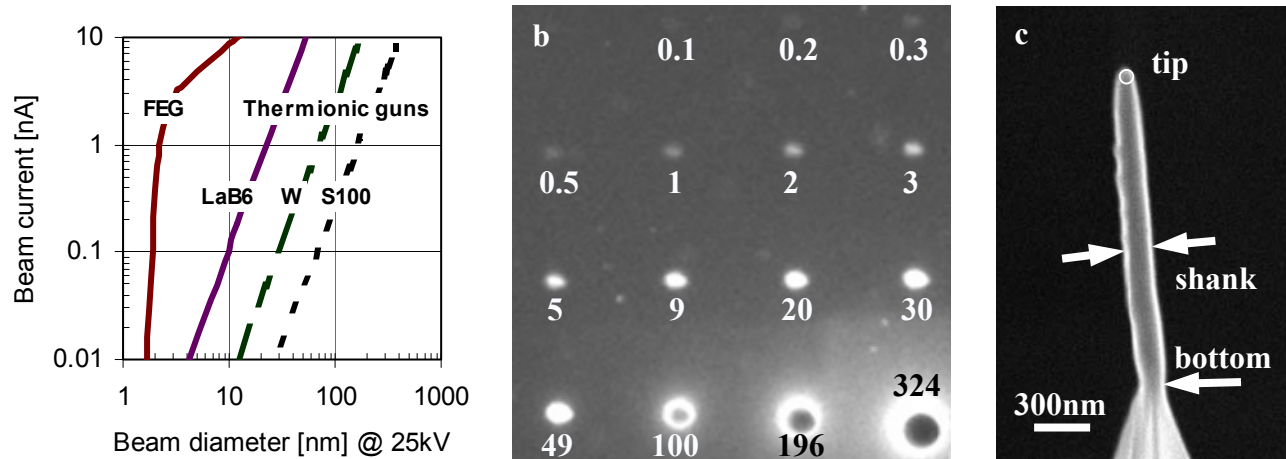


Fig. 1: Electron beam diameter ($1/e^2$) versus electron beam current for different electron gun emitters at 20-25kV (FEG: field emission gun, LaB₆: lanthanum hexaboride, W: tungsten) taken from [Reimer, 1998 #2848]. In comparison our W-emitter SEM Cambridge S100, one of the first commercially available SEMs, shows the largest beam diameter. b) Short time deposits (0.1-324s) at 25pA and 25kV of $\text{Rh}_2\text{Cl}_2(\text{PF}_3)_4$ on thin carbon film. Horizontal dot distance is 1 μm . c) Magnetic supertip from Co-carbonyl on top of pyramidal Si tip at 100pA and 25kV. Note the different diameters.

$1/e^2$) whereas the cylindrical shank diameter is about 2 times larger due to increased beam broadening with increasing penetration depth of electrons. Monte Carlo simulations show that >80% of impinging electrons exit the cylindrical deposit wall and induce additional radial growth. This effect can be avoided by depositing free-standing horizontal rods by scanning the electron beam laterally. Optimized lateral scan speeds result in deposit diameters corresponding to the beam size. However, the ultimate physical limit should be given by the escape thickness of secondary electrons in the deposit the value of which varies between 5-10nm. (for Al: 5nm [9]). The smallest ever published freestanding rods have a diameter of 15 nm and were produced in a TEM at 200 keV [10] using a tungsten precursor. Dots of Pt containing carbonaceous material with 20 nm diameter were recently obtained [11]. We can conclude that for a given beam diameter the minimum deposit dimensions depend on its geometry. For dot deposits resolution depends on aspect ratio (time), for vertical deposits on electron scattering (beam broadening) and for horizontal free standing rods on scan speed.

2 Physico-chemical limits – Growth rates – Mass transport versus electron current

For all serial processes speed is of paramount importance. FEB deposition rates up to 150nm/s are reported in literature [12]. As a localized Chemical Vapor Deposition (CVD) process FEB deposition underlies the same rules as all CVD processes; the growth rate can either be limited by the mass transport or by the chemical reaction rate. The adsorption rate dn/dt of precursor molecules can be expressed as

$$\frac{dn}{dt} = sJ \left(1 - \frac{n}{n_0} \right) - \frac{n_0}{\tau} - \sigma n f + D \nabla^2 n \quad (1)$$

with s the sticking coefficient, J the precursor flux, n_0 the monolayer density, τ the mean dwell time, σ the interaction cross section, D the diffusion coefficient and f the electron flux. The first term describes molecule adsorption as dependence of monolayer coverage, the second term desorption, the third term decomposition by electrons and the fourth term diffusion (see also fig. 2.a). Solving equation (1) for equilibrium conditions results in constant growth rates. If diffusion is neglected the steady state growth rate R is given by [5]:

$$R = v s J \left(1 + \frac{n_0 + s \tau J}{n_0 \tau \sigma f} \right)^{-1} \quad (2)$$

with v the volume of the (decomposed) molecule. It should be noted that experimentally observed deposition rates for tip deposits decrease with time.

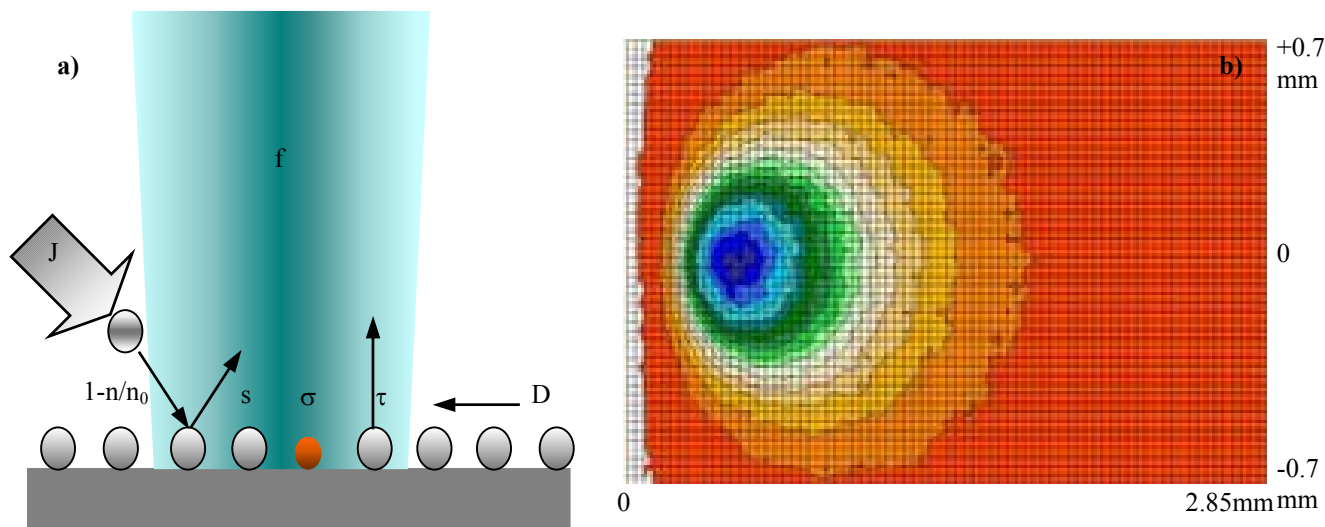


Fig. 2: a) Mechanisms determining the adsorption rate in the focused electron beam irradiated area f . Sticking, dwell time, decomposition, and coverage are symbolized, see also eq. (1). Molecule size is not at scale. b) Mapping of precursor molecules arriving from a 45° inclined micro-tube with a radius $R=285\mu\text{m}$ and a length $L/R=21$ on a horizontal substrate. The tube axis is aligned to $y=0$. Mean free path λ is $46.8\ \mu\text{m}$ and $\lambda/R=0.16$. An almost cosine distribution is obtained due to intermolecular collisions. The color code is as follows: precursor flux $J=\text{maximum}$ for black center, $J=0$ for white on the left side, color increment is 6.25% .

2.1. Precursor Effusion

An oriented tube from which the precursor effuses onto the substrate has the advantage that byproducts are more efficiently pumped away from the reaction zone. The precursor flow arriving on the substrate depends on the tube dimensions, the molecular mass of the precursor, its vapor pressure, and the vacuum chamber pressure into which the precursor effuses. The orientation (e.g. 45° angle) and position of the tube relative to the substrate surface where the electron beam impinges is also important. A schematic demonstration is given in Figure 4. Distributions of molecules impinging on the substrate are obtained from simulations for the molecular flux regime taking into account collisions between molecules [13], see fig. 2.b.

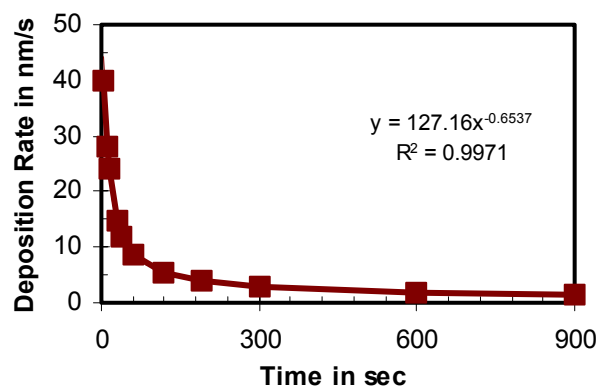
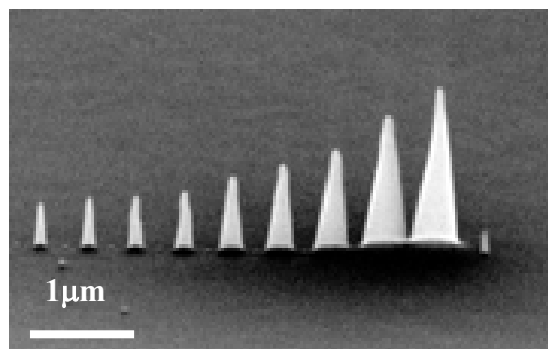


Fig. 3. : Example of surface diffusion limited deposition. Contamination deposits in a JEOL 6400 (LaB6) at 40kV , 70pA , working distance 15mm . Chamber pressure $6\text{e-}7\text{mbar}$. Note the growth of the deposit diameter at the bottom.

2.2. Precursor Diffusion

Precursor surface diffusion can be studied at contamination deposits. No precursor is supplied and deposition occurs due to decomposition of residual fragments from pump oils adsorbed onto the otherwise clean surface. In fig. 3., a series of tip deposits with varying time was performed. The deposition rate reduces drastically by about one order of magnitude at a tip height of about 400nm owing to the increasing diffusion path. The apex diameter is constant, however, the bottom diameter increases steadily due to surface diffusion into the decomposition zone.

The ratio between surface diffusion and gas phase transport during FEB deposition could be studied by varying the

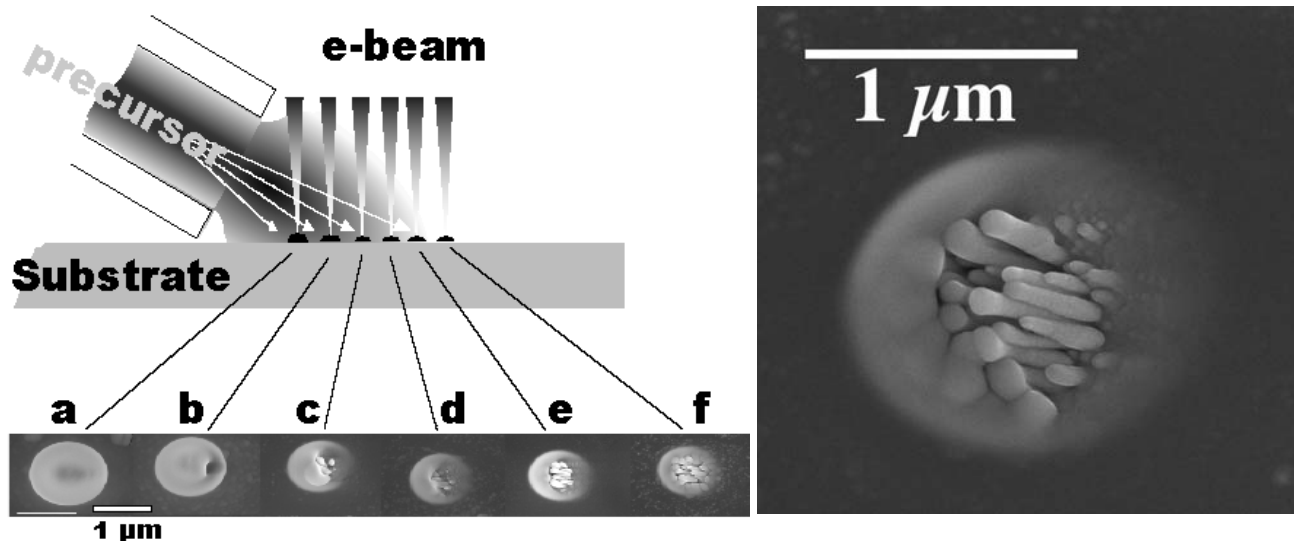


Fig. 4 : Schematic drawing of the orientation of the precursor flux onto the substrate (see also fig. 2.b) with the corresponding SEM top view pictures of FEB deposits. The deposition conditions are 25 keV acceleration voltage, as precursor: $\text{Rh}_2\text{Cl}_2(\text{PF}_3)_4$ on oxidized Si as substrate, beam current 1 nA, deposition time for every spot was 180 seconds. The distances from a to f, were 10, 150, 430, 570, 800, 1000 micrometers respectively, from the upper edge of the tube ($y=0$). The latter deposit is shown at higher magnification on the right.

distance from the tube exit, if the surface residence time of the precursor molecules were known. A decrease in deposition rate (due to a decrease in precursor flux) and a shape evolution can be monitored with increasing distance obtained with $\text{Rh}_2\text{Cl}_2(\text{PF}_3)_4$, see fig. 4. However, deposits at large distances from the tube exit (1 mm) still show features oriented to the precursor tube exit, i.e molecules impinging directly from the gas phase contribute to the deposition rate under these conditions.

For surface diffusion limited growth the vertical deposition rate is higher at low currents than at high currents. Due to the increased beam size with increasing electron current, precursor molecules are decomposed on their way to the center of the electron beam. The vertical deposition rate seems to be limited by the lateral deposition reducing the amount of precursor reaching the central part of the electron beam. In this region with highest electron densities we are always precursor transport limited.

3 Chemical decomposition reaction – Ionization - Fragmentation – Composition of deposit

The most complex and less understood part of FEB deposition is the decomposition of the adsorbed precursor molecules. The electron dissociation cross sections as function of electron energy was published by Cosby [14] for a simple compound, carbon-monoxide CO ($\sigma = 0.75 \times 10^{-16} \text{ cm}^2$ at 50eV) and for osmium carbonyl the electron dissociation cross section was estimated to be $\sigma = 0.15 \times 10^{-16} \text{ cm}^2$ from FEB deposition at 40keV [5]. However, no studies are found describing the molecular fragmentation path resulting in deposits. One of the reasons is that the amount of decomposed precursor and of deposited material is very small (picograms).

We performed quadrupole mass spectrometry measurements to determine the fragmentation path of the inorganic $\text{Rh}_2\text{Cl}_2(\text{PF}_3)_4$ precursor. The detected positively charged fragments of the electron induced ionization process show, that the dissociation of PF_3 groups is the predominant decomposition path. No fragments indicating the separation of fluorine from phosphorous were detected. These findings were confirmed by density functional theory (DFT) calculations of the decomposition of the precursor molecule [15]. However, the deposit composition determined by Auger electron spectroscopy shows up to 60 at% Rh (as 4-8 nm nano-crystals, see fig. 5 a-c) with P and Cl as main contaminants, which is in contradiction to the above measurements of electron induced fragmentation of precursor molecules in the gas phase. This fact shows, that it is very difficult to extrapolate the FEB deposit composition from mass spectrometry data. Probably surface catalyzed reactions, rearrangements, and polymerization reactions play an important role during FEB-deposition.

FEB deposition of another chemical compound of the same family, AuCIPF₃ results in deposits of almost pure gold, proven by 4-point probe measurements of highly electrically conducting gold nanowires having an electrical resistivity of 22 μΩcm, (Au: 2.4 μΩcm at room temperature). A very high nanowire resolution of 50 nm was obtained with our microscope, as can be seen in fig. 5d.

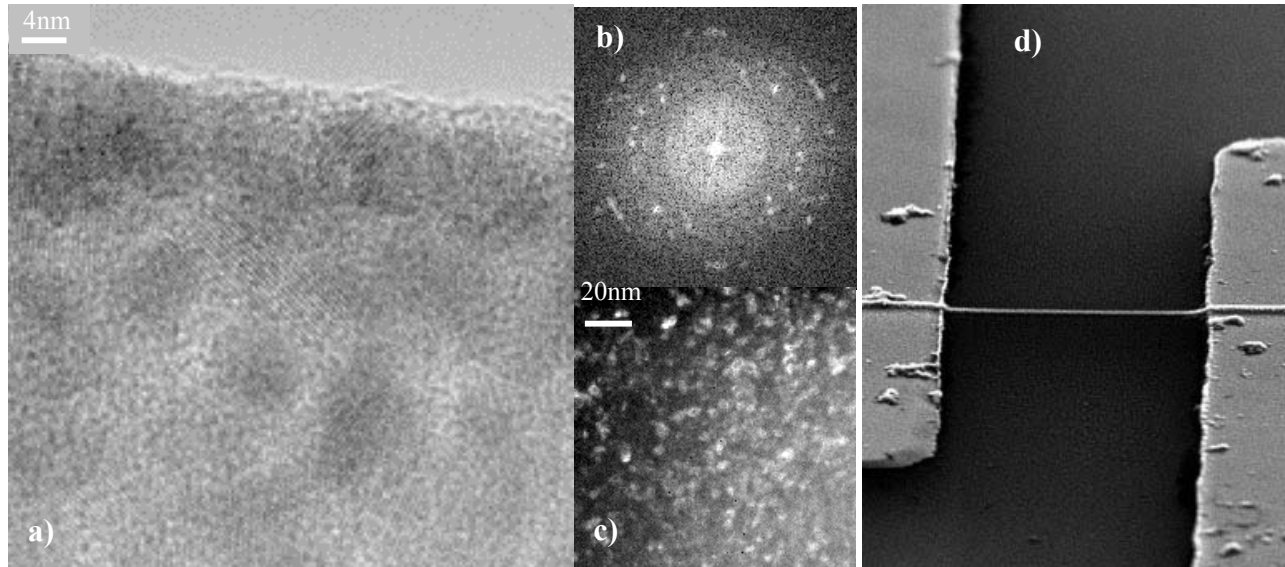


Fig. 5. : TEM images of a deposit grown with 15kV at 8nA beam current from Rh₂Cl₂(PF₃)₄: a) HRTEM image showing Rh lattice planes of nanocrystals of 4...8nm in diameter. b) Electron diffraction pattern, proving the polycrystalline nature. c) dark field image of Rh-clusters. d) Tilted SEM image of a gold line with resistivity of 22μΩcm (10x Au bulk value) deposited from AuCIPF₃. The distance of the photo-lithographically deposited gold electrodes is 5μm.

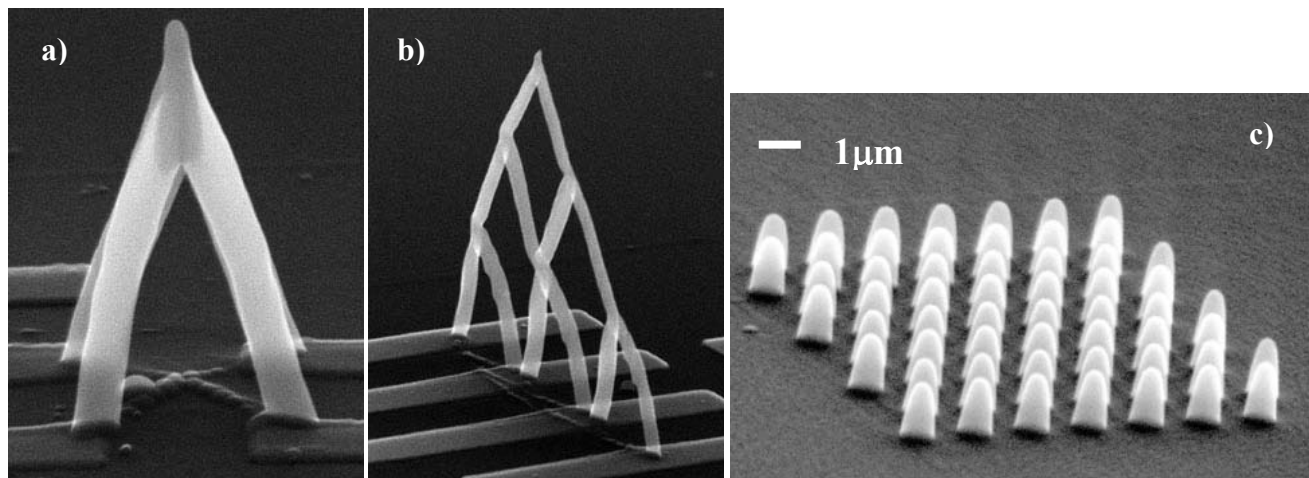


Fig. 6: a and b) 3D FEB deposits on Au electrodes from Dimethyl-hexafluoroacetylacetonate (CH₃)₂Au(hfa), fabricated by e-beam lithography and lift-off process. Distance between electrodes is 500nm. c) SEM image of hexagonal tip arrays deposited with FEB. The deposition time gives control over the tip height. Additionally, the tip inclination angle can be varied moving the electron beam with the lithography program during exposure. Tips contain about 80wt% Au and 20wt% carbon.

4 Conclusions

Focused Electron Beam (FEB) induced chemistry like deposition and etching are important processes for future rapid prototyping tools in nanotechnologies. There are many challenging applications of this extremely flexible technology, like mask and device repair in microelectronics and micro-optoelectronics, prototype production of nano-electrodes for studies in a large variety of research fields, and prototypes of nano-optical devices like 3 dimensional photonic crystal structures, see for example fig. 6. FEB deposition of other materials like magnetic Co nanoparticles (2-4 nm in diameter) embedded in an amorphous oxidation protecting carbon film, deposited on silicon cantilevers and used for high resolution magnetic force microscopy studies (see fig. 1c) present first impacts in applications. The demand for local three dimensional structuring of surfaces is increasing, and spans over a very large number of materials and functionalities.

Historically the first deposits were obtained from “contamination” in SEM or TEM machines, being condensed vapors of pump oil. The obtained deposits contain carbon, often called diamond-like carbon. Recently, we measured the mechanical properties of such deposits showing a very high elasticity modulus of 0.4 TPa, responsible for the name of the carbon deposits. In this case, not even the precursor compound is precisely known, that results in the high performing deposits. This is an example of the basic research still needed to improve the performance of FEB deposition. With the present work we tried to inform about the complexity of the FEB deposition process and the state of the art of the understanding of the ongoing processes. The influences of the physical and physico-chemical parameters of the FEB deposition process on the limiting size of deposits and growth rates of the deposits will become clear in the near future. On the other hand, the electron induced chemical fragmentation reactions are still not understood. Exceptions happen, using thermally fragile precursor molecules (decomposition temperatures below 100°C) containing noble metals, which result in high quality deposits probably due to electron induced local heating. We have shown that high deposit purity and therefore high functionality can be obtained by a proper precursor choice. But for specific tailoring of precursors for FEB deposition, the understanding of the electron beam induced chemical processes of molecules close to surfaces is still insufficient.

Acknowledgements

The authors are grateful to Benjamin Dwir (IMO/EPFL) as participant in all FEB deposition projects, Simone Amorosi and Giacomo Benvenuti (both IOA/EPFL) for the Monte Carlo simulations, Klaus Leifer (IMO/EPFL) for the TEM work, Hans-Jörg Mathieu and Nicolas Xanthopoulos (both LMCH/DMX/EPFL) for the Auger measurements, Pascal Doppelt (ESPCI, Paris) for the synthesis of the precursors, Patrick Seuret, Jacques Weber, and Thomas Wesolowski (University Geneva) for the density functional theory calculations, and EPFL, CTI and ETH-Rat financing the TOP NANO 21 program, and the Swiss National Science Foundation for financial support.

References

1. S. R. Lariviere, *Phys. Rev.*, **45**, 488-490, (1934).
2. A. E. Ennos, *Brit. J. Appl. Phys.*, **5**, 27-31, (1954).
3. S. Matsui and K. Mori, *J. Vac. Sci. Technol. B*, **4**, 299-304, (1986).
4. H. W. P. Koops, R. Weiel, D. P. Kern and T. H. Baum, *J. Vac. Sci. Technol. B*, **6**, 477-481, (1988).
5. V. Scheuer, H. Koops and T. Tschudi, *Microelectron. Engin.*, **5**, 423-430, (1986).
6. R. W. Christy, *J. Appl. Phys.*, **31**, 1680, (1960).
7. L. Reimer, *Scanning Electron Microscopy*; 2nd ed.; Springer: Berlin, Vol. 45, 1998.
8. P. Hoffmann, I. Utke, F. Ciccoira, B. Dwir, K. Leifer, E. Kapon and P. Doppelt; *Proc. Mater. Res. Soc. Spring Meeting*, **624**.171-177. (2000)
9. D. C. Joy, *Monte Carlo modeling for electron microscopy and microanalysis*; Oxford University Press: New York, 1995.
10. S. Matsui and T. Ichihashi, *Appl. Phys. Lett.*, **53**, 842-4, (1988).
11. H. W. P. Koops, 2001, personal communication
12. H. W. P. Koops, A. Kaya and M. Weber, *J. Vac. Sci. Technol. B*, **13**, 2400-2403, (1995).
13. G. Benvenuti, S. Amorosi, I. Utke, A. Luisier and P. Hoffmann, (to be published).
14. P. C. Cosby, *J. Chem. Phys.*, **98**, 7804-7818, (1993).
15. P. Seuret, J. Weber, T. Wesolowski, F. Ciccoira and P. Hoffmann, (to be published).